

# Efficient Analysis of Ferrite Loaded Waveguides Using the MRFD Method

Mesut GOKTEN

R&D and Satellite Design Department, Turksat AS, Golbasi, Ankara 06830 Turkey

mgokten@turksat.com.tr

**Abstract.** A full wave two-dimensional Multiresolution Frequency Domain formulation for efficient analysis of the dispersion characteristics of ferrite loaded waveguide structures is developed and presented. It has been concluded that the proposed formulation, which takes advantage of the compactly supported wavelet bases to expand electric and magnetic fields, allows coarser discretization compared to conventional Finite Difference Frequency Domain (FDFD) scheme. The efficiency and accuracy of the newly developed formulation, in comparison to FDFD method, is demonstrated by solving the dispersion characteristics of fully and partially ferrite loaded waveguide structures.

## Keywords

Multiresolution analysis, Finite Difference Method, MRFD, ferrite loaded waveguide, frequency domain.

## 1. Introduction

Since ferrites are magnetically anisotropic materials, their magnetic constitutive relations can be controlled by means of a DC magnetic bias field. This flexibility of ferrites makes them the choice of material in the manufacturing of non-reciprocal and control devices such as isolators, circulators and phase shifters. Numerical characterization of ferrite materials is an essential issue in the design process of these devices; hence the finite difference techniques in time domain [1], [2] and frequency domain [3] are readily used for this purpose.

The multiresolution analysis has been extensively studied in computational electromagnetics research [4-6] and it has been concluded that multiresolution analysis based techniques yield very efficient algorithms when applied to the numerical modeling of differential equations. Based on the conclusions, the Multiresolution Frequency Domain (MRFD) technique was introduced [7-9]. This technique is developed by applying Galerkin's method of moments procedure to Maxwell's curl equations while using the Cohen-Daubechies-Feauveau (CDF) [10] family of wavelets as the basis of expansion of unknown fields. CDF wavelets are a symmetric biorthogonal wavelet family

that utilizes two scaling functions due to biorthogonality. The CDF(2,2) wavelet, which is sketched in Fig. 1, is adopted for this work.

MRFD is a mathematically intensive yet computationally efficient technique, which consumes computer resources more efficiently. It has been used to model dispersion characteristics of general guided wave structures loaded with isotropic materials [11]. In this work, the 2D-MRFD technique is extended to anisotropic material modeling.

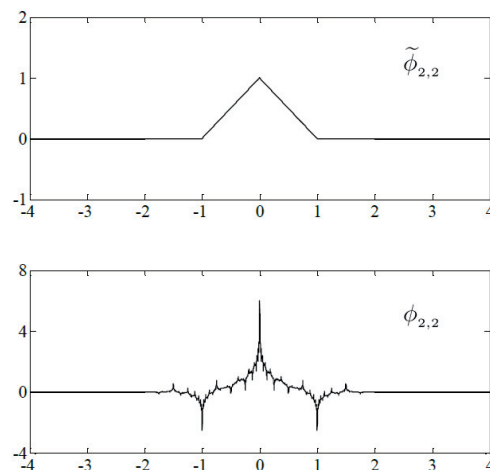


Fig. 1. Scaling functions of the CDF(2,2) wavelet base.

## 2. Formulation

### 2.1 Field Equations

Ferrite materials with diagonal dielectric constant tensors and  $y$ -directed bias magnetization are considered. For these materials, permittivity and permeability tensors can be expressed as [12]:

$$[\varepsilon] = \begin{bmatrix} \varepsilon_x & 0 & 0 \\ 0 & \varepsilon_y & 0 \\ 0 & 0 & \varepsilon_z \end{bmatrix}, \quad [\mu] = \begin{bmatrix} \mu & 0 & j\kappa \\ 0 & \mu_0 & 0 \\ -j\kappa & 0 & \mu \end{bmatrix}. \quad (1)$$

where

$$\mu = \mu_0 \left( 1 + \frac{\omega_m (\omega_0 + j\omega\alpha)}{(\omega_0 + j\omega\alpha)^2 - \omega^2} \right) \quad (2)$$

$$\kappa = \mu_0 \frac{\omega\omega_m}{(\omega_0 + j\omega\alpha)^2 - \omega^2} \quad (3)$$

$$\omega_m = \gamma_m M_s \quad (4)$$

$$\omega_0 = \gamma_m H_0 \quad (5)$$

Here  $\gamma_m = -2.21042 \times 10^5$  (rad/s)/(A/m) is the gyro-magnetic ratio,  $\alpha$  is the damping factor,  $M_s$  and  $H_0$  are DC magnetic saturation and magnetic bias, respectively.

Assuming that the waveguiding structure is uniform along the  $z$  axis and the wave is propagating in the positive  $z$  direction, the electric and magnetic fields inside the guided wave structure can be expressed as:

$$\vec{E}(x, y, z) = [E_x(x, y)\hat{x} + E_y(x, y)\hat{y} + E_z(x, y)\hat{z}]e^{-j\beta z} \quad (6.a)$$

$$\vec{H}(x, y, z) = [H_x(x, y)\hat{x} + H_y(x, y)\hat{y} + H_z(x, y)\hat{z}]e^{-j\beta z} \quad (6.b)$$

where  $\beta$  is the propagation constant.

Substituting (6) into Maxwell's curl and divergence equations and replacing the space derivatives with respect to  $z$  by  $-j\beta$ , the following scalar equations are obtained:

$$\beta E_x(x, y) = \omega\mu_0 H_y(x, y) + j \frac{\partial E_z(x, y)}{\partial x} \quad (7.a)$$

$$\beta E_y(x, y) = -\omega\mu H_x(x, y) - j\omega\kappa H_z(x, y) + j \frac{\partial E_z(x, y)}{\partial y} \quad (7.b)$$

$$\beta H_x(x, y) = -\omega\varepsilon_y E_y(x, y) + j \frac{\partial H_z(x, y)}{\partial x} \quad (7.c)$$

$$\beta H_y(x, y) = \omega\varepsilon_x E_x(x, y) + j \frac{\partial H_z(x, y)}{\partial y} \quad (7.d)$$

$$\beta E_z(x, y) = -j \frac{\varepsilon_x}{\varepsilon_z} \frac{\partial E_x(x, y)}{\partial x} - j \frac{\varepsilon_y}{\varepsilon_z} \frac{\partial E_y(x, y)}{\partial y} \quad (7.e)$$

$$\beta H_z(x, y) = -j\omega\varepsilon_y \frac{\kappa}{\mu} E_y(x, y) - j \frac{\partial H_x(x, y)}{\partial x} - j \frac{\mu_0}{\mu} \frac{\partial H_y(x, y)}{\partial y} \quad (7.f)$$

## 2.2 MRFD Equations

The MRFD equations for (7.a), (7.c), (7.d) and (7.e) are provided in [10], however due to the extra terms in (7.b) and (7.f), MRFD equations for these should be derived. Derivation procedure is similar to the one provided in [10]. Derivation starts with the expansion of the unknown fields in terms of the dual scaling functions and inserting the expansions into field equations. The resulting

equation is then sampled with the scaling function according to Galerkin's method.

Derivation of the MRFD equation for (7.b) is provided below. Derivation starts with the expansion of the unknown fields in terms of the dual scaling functions of the CDF (2,2) wavelet, such that:

$$E_x(x, y) = \sum_{i', j'} E_x(i', j') \tilde{\phi}_{i'+1/2}(x) \tilde{\phi}_{j'}(y) \quad (8.a)$$

$$E_y(x, y) = \sum_{i', j'} E_y(i', j') \tilde{\phi}_{i'}(x) \tilde{\phi}_{j'+1/2}(y) \quad (8.b)$$

$$E_z(x, y) = \sum_{i', j'} E_z(i', j') \tilde{\phi}_{i'}(x) \tilde{\phi}_{j'}(y) \quad (8.c)$$

$$H_x(x, y) = \sum_{i', j'} H_x(i', j') \tilde{\phi}_{i'}(x) \tilde{\phi}_{j'+1/2}(y) \quad (8.d)$$

$$H_y(x, y) = \sum_{i', j'} H_y(i', j') \tilde{\phi}_{i'+1/2}(x) \tilde{\phi}_{j'}(y) \quad (8.e)$$

$$H_z(x, y) = \sum_{i', j'} H_z(i', j') \tilde{\phi}_{i'+1/2}(x) \tilde{\phi}_{j'+1/2}(y) \quad (8.f)$$

Function  $\tilde{\phi}_n(x)$  is the scaled and shifted CDF dual scaling function  $\phi(x)$  defined as:

$$\tilde{\phi}_n(x) = \tilde{\phi}\left(\frac{x - n\Delta x}{\Delta x}\right). \quad (9)$$

The locations of the scaling functions, indicated by indexes  $i, j$  in the above expansions, correspond to the locations of the field components on the compact 2D grid shown in Fig. 2. This grid structure is obtained simply by collapsing the 3D Yee cell in the  $z$  direction.

After the expansions are inserted to (7.b), the sampling procedure starts with testing the left-hand side of the resulting equation with  $\phi(x) \phi_{j+1/2}(x)$ :

$$\begin{aligned} & \int_{-\infty}^{\infty} \int_{-\infty}^{\infty} \beta E_y(x, y) \phi_i(x) \phi_{j+1/2}(y) dx dy \\ &= \beta \int_{-\infty}^{\infty} \int_{-\infty}^{\infty} \sum_{i', j'} E_y(i', j') \tilde{\phi}_{i'}(x) \tilde{\phi}_{j'+1/2}(y) \phi_i(x) \phi_{j+1/2}(y) dx dy \\ &= \beta E_y(i, j) \Delta x \Delta y. \end{aligned} \quad (10)$$

where  $\phi_n(x)$  is the scaled and shifted CDF scaling function  $\phi(x)$  defined similar to (9).

Next, the first term on the righthand side of (7.b) is tested:

$$\begin{aligned} & \int_{-\infty}^{\infty} \int_{-\infty}^{\infty} -\omega\mu H_x(x, y) \phi_i(x) \phi_{j+1/2}(y) dx dy \\ &= -\omega\mu \int_{-\infty}^{\infty} \int_{-\infty}^{\infty} \sum_{i', j'} H_x(i', j') \tilde{\phi}_{i'}(x) \tilde{\phi}_{j'+1/2}(y) \phi_i(x) \phi_{j+1/2}(y) dx dy \\ &= -\omega\mu \Delta x \Delta y H_x(i, j). \end{aligned} \quad (11)$$

The second-term on the right-hand side of (7.b) is sampled to yield:

$$\begin{aligned} & \int_{-\infty}^{\infty} \int_{-\infty}^{\infty} -j\omega\kappa H_z(x, y) \phi_i(x) \phi_{j+1/2}(y) dx dy \quad (12) \\ &= -j\omega\kappa \int_{-\infty}^{\infty} \int_{-\infty}^{\infty} \sum_{i', j'} H_z(i', j') \tilde{\phi}_{i'+\frac{1}{2}}(x) \tilde{\phi}_{j'+\frac{1}{2}}(y) \phi_i(x) \phi_{j+\frac{1}{2}}(y) dx dy \\ &= -j\omega\kappa \sum_{i', j'} H_z(i', j') \int_{-\infty}^{\infty} \tilde{\phi}_{i'+\frac{1}{2}}(x) \phi_i(x) dx \int_{-\infty}^{\infty} \tilde{\phi}_{j'+\frac{1}{2}}(y) \phi_{j+\frac{1}{2}}(y) dy \\ &= -j\omega\kappa \Delta x \Delta y \sum_{l=0}^2 b(l) [H_z(i+l, j) + H_z(i-l-1, j)] \end{aligned}$$

where

$$b(l) = \frac{1}{\Delta x} \int_{-\infty}^{\infty} \tilde{\phi}_{i+1/2+l}(x) \phi_i(x) dx. \quad (13)$$

The  $b(l)$  coefficients are given in Tab. 1. Due to symmetry of the wavelet base  $b(-1-l) = b(l)$ .

Finally, the last term on the right-hand side of (7.b) is sampled to yield:

$$\begin{aligned} & \int_{-\infty}^{\infty} \int_{-\infty}^{\infty} j \frac{\partial E_z(x, y)}{\partial y} \phi_i(x) \phi_{j+1/2}(y) dx dy \quad (14) \\ &= j \int_{-\infty}^{\infty} \int_{-\infty}^{\infty} \frac{\partial}{\partial y} \left[ \sum_{i', j'} E_z(i', j') \tilde{\phi}_{i'}(x) \tilde{\phi}_{j'}(y) \right] \phi_i(x) \phi_{j+\frac{1}{2}}(y) dx dy \\ &= j \sum_{i', j'} E_z(i', j') \int_{-\infty}^{\infty} \tilde{\phi}_{i'}(x) \phi_i(x) dx \int_{-\infty}^{\infty} \frac{\partial \tilde{\phi}_{j'}(y)}{\partial y} \phi_{j+\frac{1}{2}}(y) dy \\ &= j \Delta x \sum_{l=1}^3 a(l) [E_z(i, j+l) - E_z(i, j-l+1)]. \end{aligned}$$

where

$$a(l) = \int_{-\infty}^{\infty} \frac{\partial \tilde{\phi}_{j'+l}(y)}{\partial y} \phi_{j+1/2}(y) dy. \quad (15)$$

The  $a(l)$  coefficients are given in Tab. 1. Due to symmetry of the wavelet base  $a(-l) = -a(l+1)$ .

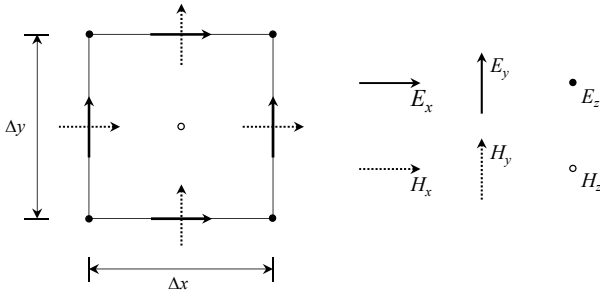


Fig. 2. 2D compact unit cell.

$L$	0	1	2
$a(l)$	1.2291667	-0.0937500	0.0104167
$b(l)$	0.5625	-0.0625	1.05e-18

Tab. 1. The  $a(l)$  and  $b(l)$  coefficients.

Substituting (10), (11), (12) and (14) into (7.b) yields the MRFD equation:

$$\begin{aligned} \beta E_y(i, j) &= \\ & -\omega\mu H_x(i, j) \\ & -j\omega\kappa \sum_{l=0}^2 b(l) [H_z(i+l, j) + H_z(i-l-1, j)] \quad (16) \\ & + j \sum_{l=1}^3 a(l) \frac{E_z(i, j+l) - E_z(i, j-l+1)}{\Delta y}. \end{aligned}$$

The MRFD equation for (7.f) can be obtained similarly:

$$\begin{aligned} \beta H_z(i, j) &= \\ & -j\omega\epsilon_y \frac{\kappa}{\mu} \sum_{l=0}^2 b(l) [E_y(i-l, j) + E_y(i+l+1, j)] \\ & -j \sum_{l=1}^3 a(l) \frac{H_x(i+l, j) - H_x(i-l+1, j)}{\Delta x} \quad (17) \\ & -j \frac{\mu_0}{\mu} \sum_{l=1}^3 a(l) \frac{H_y(i, j+l) - H_y(i, j-l+1)}{\Delta y}. \end{aligned}$$

MRFD equations can be used to form an eigen-value problem as:

$$[A] \cdot x = \beta [I] \cdot x \quad (18)$$

where  $[A]$  is a sparse coefficient matrix,  $[I]$  is the unit matrix and  $x$  is the unknown field vector. The eigenvalues of  $[A]$  deliver the propagation constant and eigenvectors of  $[A]$  deliver the corresponding electromagnetic fields. In this work, an iterative technique called IRAM (Implicitly Restarted Arnoldi Method) [13] is used to compute the eigenvalues of  $[A]$ .

### 2.3 Boundary Conditions

In order to satisfy the boundary conditions on the perfect electric conductor (PEC)-ferrite interface, tangential electric fields and normal magnetic flux density should be set to zero. Conventional FDFD scheme can easily model the PEC boundary owing to the localized scaling function. Multiresolution schemes, however, are non-localized in nature because of the wider support of scaling functions, so they cannot support localized boundary conditions. This aspect of multiresolution schemes is the consequence of the fact that the MRFD equations of the grid nodes in the vicinity of the boundary include field components outside of the computational domain.

To demonstrate the problem, consider the PEC boundary on the left wall of the waveguide, as shown in Fig. 3. In this figure, the two leftmost cells are outside of the computational domain and consequently fields on these regions are unknown. MRFD equation (17) for  $H_z$  on the boundary cell  $(0, j)$  requires unknown field components such as  $H_x(-1, j)$ ,  $H_x(-2, j)$ ,  $E_y(-1, j)$  and  $E_y(-2, j)$ . In order to tackle this problem, multiresolution based techniques utilize the image principle [14] for modeling PEC boundary, which requires symmetry of fields around such boundary.

Because of the lack of symmetry of the magnetic fields at the ferrite-PEC boundary, image principle is not suitable to model such interface. In this work, FDFD equations of [3] are used at the boundary cells and MRFD equations are used elsewhere.

Even though FDFD equations are utilized at the boundary, MRFD equations are still used at the cells neighboring the boundary cells and similarly, MRFD equation (17) for  $H_z$  on cell  $(1, j)$  requires unknown field components such as  $H_x(-1, j)$  and  $E_y(-1, j)$ . Since  $E_y$  is zero on the left waveguide wall, image principle can be implemented by forcing odd symmetry in the form of:

$$E_y(-1, j) = -E_y(1, j). \tag{19}$$

$H_x(-1, j)$  is not zero on the PEC boundary so symmetry conditions don't apply. Instead, extrapolation can be used to solve  $H_x(-1, j)$  as:

$$H_x(-1, j) = 2H_x(0, j) - H_x(1, j). \tag{20}$$

Finally, inserting (19) and (20) into (17) yields the MRFD equation for  $H_z(1, j)$ . Similarly, boundary conditions for all equations and PEC walls are developed.

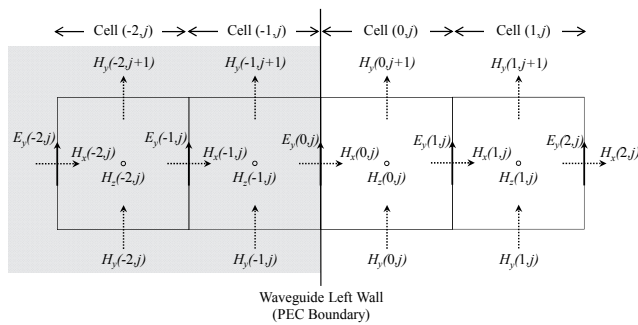


Fig. 3. 2D grid on the left wall.

### 3. Numerical Results

In order to validate the proposed MRFD formulation, two waveguide structures are analyzed. First example is a completely ferrite loaded waveguide with dielectric constant  $\epsilon_r = 9$ , damping factor  $\alpha = 0.02$ ,  $H_0 = 15915.5$  A/m,  $M_S = 159155$  A/m,  $x$ -dimension of 22.86 mm and  $y$ -dimension of 10.16 mm, shown in Fig. 4. This structure is analyzed with both the FDFD [3] and MRFD techniques and phase constant of the dominant  $TE_{10}$  mode, as shown in Fig. 5 is calculated. The simulation results are compared to the exact results [12] and it is observed that the agreement between MRFD, FDFD and exact solution is almost perfect. The grid size, matrix size and simulation time for both FDFD and MRFD simulations are summarized in Tab. 2. For this case, compared to FDFD, MRFD scheme utilized a coarser grid by a factor of three and consumed 45% less memory and 72.6% less simulation time while achieving a competitive accuracy.

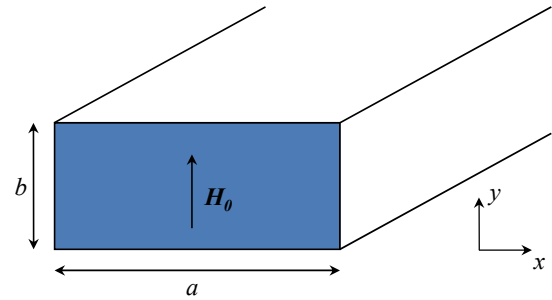


Fig. 4. Uniformly ferrite loaded waveguide.

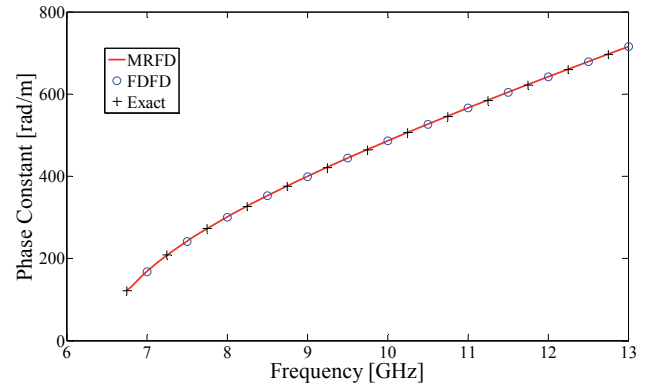


Fig. 5. Phase constant of the uniformly ferrite loaded waveguide.

		Grid size	Matrix Size [byte]	Time [sec]
Uniform Waveguide	FDFD	15x1	3736	3.25
	MRFD	5x1	2056	0.89
Partially Loaded Waveguide	FDFD	15x1	3736	4.20
	MRFD	6x1	2560	1.38

Tab. 2. Simulation parameters and computer resources consumed by the two methods.

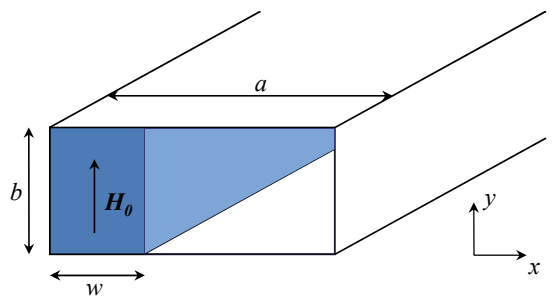


Fig. 6. Partially ferrite loaded waveguide.

The second example is a rectangular waveguide with dimensions  $a = 22.86$  mm,  $b = 10.16$  mm as shown in Fig. 6. This waveguide is partially loaded with a ferrite material of width  $w = a/3$ , dielectric constant  $\epsilon_r = 9$ , damping factor  $\alpha = 0.02$ ,  $H_0 = 15915$  A/m,  $M_S = 159150$  A/m. This type of structure allows the propagation of forward and backward waves with different propagation constants. This structure is again analyzed with both the FDFD [3]

and MRFD techniques and phase constants of the dominant TE<sub>10</sub> mode are calculated. The simulation results are then compared to the exact results [12] in Fig. 7. Very good agreement between the simulation results and exact results is noticed. Simulation parameters are summarized in Tab. 2. It is observed that for this case, in comparison to FDFD, MRFD scheme utilized a 2.5 times coarser lattice and consumed 31% less memory and 67% less simulation time while achieving similar accuracy.

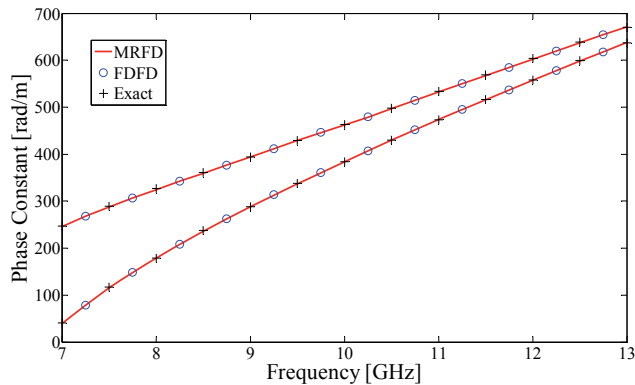


Fig. 7. Phase constant of the partially ferrite loaded waveguide. Forward phase constant at the bottom and backward phase constant on the top.

## 4. Conclusions

In this study, the CDF wavelet based multiresolution frequency domain scheme is extended to the analysis of ferrite loaded waveguide structures. In order to overcome the difficulty of modeling PEC-Ferrite interface, FDFD equations are used on the boundary cells and a combination of image principle and extrapolation technique is utilized at the boundary region.

Dispersion characteristics of fully and partially ferrite loaded waveguide structures are analyzed in order to validate the newly developed formulation. Simulation results are compared to the FDFD simulations and exact calculations. It is observed that while achieving similar accuracy, MRFD scheme utilized coarser grids by factors of 3 and 2.5 for uniform and non-uniform cases respectively, compared to FDFD. Utilizing coarser grids yielded significant savings in favor of the MRFD scheme in memory requirement and simulation time.

## Acknowledgements

The author would like to thank Dr. Ahmet F. Yagli for his support and proofreading the paper.

## References

[1] OKONIEWSKI, M., OKONIEWSKA, E. FDTD analysis of magnetized ferrites: A more efficient algorithm. *IEEE Microwave and Guided Wave Letters*, 1994, vol. 4, no. 6, p. 169 - 171.

- [2] PEREDA, J. A., VIELVA, L. A., SOLANO, M. A., VEGAS, A., PRIETO, A. FDTD analysis of magnetized ferrites. Application to the calculation of dispersion characteristics of ferrite-loaded waveguides. *IEEE Transactions on Microwave Theory and Techniques*, 1995, vol. 43, no. 2, p. 350.
- [3] AL-BARQAWI, H., DIB, N., KHODIER, M. A two-dimensional full-wave finite-difference frequency-domain analysis of ferrite loaded structures. *International Journal of Infrared and Millimeter Waves*, 2008, vol. 29, no. 5, p. 443 - 456.
- [4] ROBERTSON, R., TENTZERIS, M., KRUMPHOLZ, M., KATEHI, L. P. B. Modelling of dielectric cavity structures using multiresolution time-domain analysis. *International Journal of Numerical Modelling: Electronic Networks, Devices and Fields*, 1998, vol. 11, p. 55 -68
- [5] FUJII M., HOEFER, W. J. R. A wavelet formulation of the finite-difference method: Full-vector analysis of optical waveguide junctions. *IEEE Journal of Quantum Electronics*, 2001, vol. 37, no. 8, p. 1015-1029.
- [6] DOGARU, T., CARIN, L. Multiresolution time-domain using CDF biorthogonal wavelets. *IEEE Transactions on Microwave Theory and Techniques*, 2001, vol. 49, no. 5, p. 902-912.
- [7] GOKTEN, M., ELSHERBENI, A. Z., ARVAS, E. Electromagnetic scattering analysis using the two-dimensional MRFD formulation. *Progress in Electromagnetics Research*, 2008, vol. 79, p. 404 - 416.
- [8] GOKTEN, M., ELSHERBENI, A. Z., ARVAS, E. A multiresolution frequency domain method using biorthogonal wavelets. In *22nd Annual Review of Progress in Applied Computational Electromagnetics*. Miami, (U.S.A.), 2006, p. 16-21.
- [9] YAGLI, A. F. MRFD method for scattering from three dimensional dielectric bodies. *Radio Engineering*, Sept. 2001, vol. 20, no. 3, p. 581-586.
- [10] DAUBECHIES, I. *Ten Lectures on Wavelets*. Philadelphia, PA: Society for Industrial and Applied Mathematics, 1992.
- [11] GOKTEN, M., ELSHERBENI, A. Z., ARVAS, E. The multiresolution frequency domain method for general guided wave structures. *Progress in Electromagnetics Research*, 2007, vol. 69, p. 55-66.
- [12] POZAR, D. M. *Microwave Engineering*. 3<sup>rd</sup> ed. John Wiley, 2005.
- [13] LEHOUCQ, R. B., SORENSEN, D. C., YANG, C. *ARPACK Users' Guide: Solution of Large-Scale Eigenvalue Problems with Implicitly Restarted Arnoldi Methods*, SIAM, 1998
- [14] KRUMPHOLZ, M., KATEHI, L. P. B. MRTD: new time-domain schemes based on multiresolution analysis. *IEEE Trans. on Microwave Theory and Techniques*, 1996, vol. 44, no. 4, p. 555 -571.

## About Authors ...

**Mesut GOKTEN** was born in Tokat, Turkey in 1975. He graduated from Istanbul Technical University Electronics and Communications Engineering Dept. in 1997. He received his M.S.E.E. (with honors) and Ph.D. degrees from Syracuse University Electrical Engineering Dept. in 2003 and 2007, respectively and served as a teaching and research assistant from August 2000 to May 2005 at the same department. He was with Dielectric Laboratories, Inc of Cazenovia, NY from May 2005 to August 2006. He currently works at the R&D and Satellite Dept. at Turksat AS, Ankara, Turkey. His research is focused on computational electromagnetics, design and implementation of microwave devices and systems for satellite communications.